

HEAT FLUX MODELING IN WALL-BOUNDED TURBULENT FLOWS BY REYNOLDS STRESS MODELS WITHIN RANS AND SENSITIZED-RANS FRAMEWORKS

Maximilian Bopp, Sebastian Wegt, Louis Krüger, Suad Jakirlić

Institute of Fluid Mechanics and Aerodynamics, Technical University of Darmstadt
Alarich-Weiss-Str. 10, 64287 Darmstadt, Germany
bopp@sla.tu-darmstadt.de, jakirlic@sla.tu-darmstadt.de

Francesco Secchi, Bettina Frohnafel

Institute of Fluid Mechanics, Karlsruhe Institute of Technology (KIT)
Kaiserstrasse 10, 76131 Karlsruhe, Germany
francesco.secchi@kit.edu, bettina.frohnafel@kit.de

ABSTRACT

A comparative assessment of different modeling approaches for the heat flux $\overline{u'_j \theta'}$, with the gradient of which representing the turbulence-related heat source in the temperature transport equation, is in focus of the present computational study. The convective heat transfer under consideration takes place within two benchmark configurations: a fully-developed channel flow and a pipe-discharging jet impinging perpendicularly onto a heated wall. The heat flux models' performance is investigated in conjunction with a conventional Reynolds-stress model and its scale-resolving variant employed within a time-accurate RANS (Reynolds-Averaged-Navier-Stokes) simulation. In the Sensitized-RANS framework employing the scale-resolving Improved Instability-Sensitive Reynolds Stress Model (IISRSM) (Jakirlić & Maduta (2015)), the turbulent correlations are employed within the set of relevant momentum equations as 'sub-scale' quantities. The scalar flux models represent the so-called gradient approach with the diffusion-like coefficient formulated in terms of both eddy-viscosity and the full Reynolds stress tensor. The IISRSM-related 'sub-scale' turbulent length and time scales constituting these relationships are determined by utilizing the unresolved residual part of the entire anisotropic sub-scale Reynolds-stress tensor, as well as the corresponding turbulence kinetic energy and its viscous dissipation rate.

INTRODUCTION

A crucial disadvantage of heat transfer predictions when using Reynolds-Averaged Navier-Stokes (RANS) models is their lack of accuracy in even weakly complex flow configurations. Even in conjunction with the models accounting for the near-wall turbulence, the majority of the wall heat transfer models fails to capture correctly the heat transport in the diffusive sub-layer and the thermal buffer layer, Šarić & Basara (2018). The influence of modeled heat transport in RANS simulations is therefore of great importance. Even the heat transfer studies in simpler flow configurations with exclusively gaseous media by using near-wall turbulence models are often reported to deliver wrong Nusselt number predictions compared to corresponding experimental data, Chang & Shyu (2000). A com-

mon underlying problem seems to be the variation of the turbulent Prandtl number (Pr_t) in the wall proximity, which is not at all accounted for, e.g., in the most-widely used model formulation for $\overline{u'_j \theta'}$, the so-called gradient diffusion approach - representing the straightforward proportionality to the mean temperature gradient - in conjunction with the Boussinesq approximation:

$$-\overline{u'_j \theta'} = \alpha_t \frac{\partial \Theta}{\partial x_j} \quad \text{with} \quad \alpha_t = \frac{\nu_t}{Pr_t} \quad (1)$$

Here, the eddy diffusivity of the temperature field α_t is expressed commonly in terms of the eddy viscosity ν_t and the constant turbulent Prandtl number Pr_t . This kind of formulation leads actually to another major weakness: a simple formulation like this is not capable of capturing turbulence anisotropy residing in modeled diffusive fluxes due to the scalar nature of the eddy viscosity. Accordingly, not the Reynolds stress component being mostly affected by the wall proximity is going to be applied within this proportionality coefficient, but the entire turbulence kinetic energy ($k = 0.5\overline{u'_i u'_i}$). The present work focuses therefore on studying various algebraic expressions for the heat flux correlation $-\overline{u'_j \theta'}$ aiming at a comparative assessment of their predictive performances with respect to the resulting near-wall temperature field and associated Nusselt number distributions. This background model of turbulence is a near-wall Reynolds stress model applied in the context of both computational frameworks, the conventional RANS and the so-called sensitized, eddy-resolving RANS approach (Jakirlić & Maduta (2015)).

COMPUTATIONAL MODEL

The equations of motion governing the underlying incompressible velocity field within an unsteady conventional/sensitized RANS framework read:

$$\frac{\partial}{\partial t} (\overline{U}_i) + \overline{U}_j \frac{\partial (\overline{U}_i)}{\partial x_j} = \frac{\partial}{\partial x_j} \left[\nu \left(\frac{\partial \overline{U}_i}{\partial x_j} \right) - \overline{u'_i u'_j} \right] \quad (2)$$

The Reynolds-stress tensor $\overline{u'_i u'_j}$, mimicking the subscale stress tensor in this RANS-based eddy-resolving method, is determined by a second-moment closure formulation by solving the following transport equation:

$$\frac{D\overline{u'_i u'_j}}{Dt} = P_{ij} + \Phi_{ij} - \varepsilon_{ij}^h + \frac{\partial}{\partial x_k} (0.5D_{ij}^v + D_{ij}^u) \quad (3)$$

The source terms on the RHS of the Reynolds-stress transport equation describe the exactly treated production rate P_{ij} , the redistribution process Φ_{ij} , the viscous dissipation correlation ε_{ij} and various diffusion processes $D_{ij}^{(v+u)}$. The molecular diffusion D_{ij}^v , similar as the production rate P_{ij} , is to be exactly treated; all other processes have to be adequately modeled. Unlike a conventional RANS Reynolds-stress model, being incapable of describing any spectral dynamics of the turbulence field, the presently utilized IIS-RSM, representing its scale-resolving version, is appropriately sensitized towards adequate capturing of turbulent fluctuations. The latter feature is introduced along with the SAS (Scale-Adaptive Simulation) methodology, proposed by Menter & Egorov (2010). The IIS-RSM model accounts for an additional production term which is introduced into the equation governing the specific homogeneous dissipation rate $\omega^h = \varepsilon^h/k$, with $\varepsilon^h = \varepsilon - 0.5D_k^v$ and $k = 0.5\overline{u_i u_i}$.

$$\left(\frac{D\omega^h}{Dt}\right)_{IIS-RSM} = \left(\frac{D\omega^h}{Dt}\right)_{RSM} + P_{IIS-RSM} \quad (4)$$

The inference of the model is its self-adjustment to the scales residing in the unresolved residual motion, by interplaying with the underlying grid resolution, Menter & Egorov (2010). Herewith, the development of turbulent fluctuations is enabled. Unlike the initial SAS proposal employing the von Karman length scale ($L_{vK} \propto \nabla U_i / \nabla^2 U_i$) as a triggering parameter to enable the resolving mode, the presently utilized term is modeled only in terms of the second velocity derivative ($\nabla^2 U_i$), as originated from the equation governing the integral length scale, Rotta (1972). By doing so the sensitivity of the model in capturing the turbulence fluctuations is enhanced enabling the use of coarser grid resolutions.

The temperature equation used resembles the most common form of the energy equation for an ideal gas with constant heat capacities, thermal conductivity and density, small temperature variations and without consideration of thermal radiation (Chang & Shyu (2000)):

$$\frac{\partial(\overline{\Theta})}{\partial t} + \overline{U_j} \frac{\partial(\overline{\Theta})}{\partial x_j} = \frac{\partial}{\partial x_j} \left(\frac{v}{Pr} \frac{\partial \overline{\Theta}}{\partial x_j} - \overline{u'_j \theta'} \right) \quad (5)$$

The turbulent heat flux $-\overline{u'_j \theta'}$ is commonly modeled by the so-called SGDH formulation (Simple Gradient Diffusion Hypothesis). In models of this type, the scalar fluxes are related to the mean scalar-field gradients via a scalar turbulent diffusivity (Γ_t).

$$-\overline{u'_j \theta'} = \Gamma_t \frac{\partial \overline{\Theta}}{\partial x_j} \quad \text{with} \quad \Gamma_t = \frac{v_t}{Pr_t} \quad \text{or} \quad \Gamma_t = \frac{C_\mu k^2}{Pr_t \varepsilon} \quad (6)$$

As it is well-known the models of this type, commonly applied in terms of a constant Prandtl number, result in a poor

outcome in even simple flow configurations. The absence of an explicit dependence on the Reynolds stresses $\overline{u'_i u'_j}$ makes these models incapable of dealing with turbulence anisotropy, which is especially pronounced in the wall vicinity. Accordingly, the isotropic nature of the turbulent diffusivity implies obvious alignment of the turbulent scalar flux and the mean scalar gradient. This is clearly not the case in any complex flow configuration. A more extensive closure formulation is in focus of the present modeling activities, representing a generalization towards the gradient-transport hypothesis by using a turbulent diffusivity tensor D_{ij} (see e.g. Abe & Suga (2001)):

$$-\overline{u'_i \theta'} = D_{ij} \frac{\partial \overline{\Theta}}{\partial x_j} \quad (7)$$

with

$$D_{ij} = k\tau \left(C_{\theta,1} \frac{\overline{u'_i u'_j}}{k} + C_{\theta,2} \frac{\overline{u'_i u'_k} \overline{u'_k u'_j}}{k^2} \right) \quad (8)$$

with $\tau = k/\varepsilon^h$ representing the turbulent time scale. In the case of $C_{\theta,2} = 0$ the model reduces to the well-known General-Gradient Diffusion Hypothesis (GGDH). The above model is an anisotropy-reflecting algebraic model capable of dealing with complex flow straining.

CASE DESCRIPTION AND COMPUTATIONAL DETAILS

The presently considered flow configurations are concerned with the convective heat transfer in a fully-developed channel flow at $Re_\tau = 180$ (reference DNS by Horiuti (1992) and Kasagi *et al.* (1992)) and a round impinging jet onto a smooth, heated wall at $Re = 10000$ (reference DNS by Secchi *et al.* (2022)).

The Reynolds stress model equations are implemented into the finite-volume-based open source toolbox OpenFOAM® (Open Source Field Operation and Manipulation) with which all simulations are performed. Both the conventional Reynolds-stress model and its instability-sensitized version (Jakirlić & Maduta (2015), see also Jakirlić & Maduta (2016)) are applied in the time-accurate RANS framework. The background model formulation is based on the so-called homogeneous dissipation rate concept, proposed by Jakirlić & Hanjalić (2002). A controlled adaptive time step ensures a Courant number smaller than one in the entire solution domain. The discretization of the convective terms in the momentum and temperature equations is performed by applying the 2nd order accurate Central Differencing Scheme (CDS). The flow domain is meshed by using the OpenFOAM's mesh utility denoted as 'blockMesh'. The mesh is generated with an appropriate grading towards the walls, providing the wall-next computational node situated well within the viscous sub-layer, exhibiting a dimensionless wall distance y^+ substantially smaller than one. This is especially important for the correct calculation of the sub-scale heat flux in the immediate wall proximity.

Fig. 1 illustrates schematically the convective heat transfer within a fully-developed channel flow. The uniform temperature profile over the channel cross-section is introduced into the flow and subjected to continuous heat removal through the walls by a constant heat flux, leading to a constant temperature value at both walls. The solution domain adopted for the

Sensitized RANS simulations with the IIS-RSM corresponds typically to a regular hexahedron, confined by bottom and upper walls, with the dimensions $L_x \times L_y \times L_z = 2\pi h \times 2h \times \pi h$ and h representing the channel half height. The relevant numerical mesh consists of $N_x \times N_y \times N_z = 60 \times 64 \times 32$ cells, resulting in 122880 cells in total. The conventional RANS computations are performed on a two-dimensional flow domain ($L_x \times L_y = 2\pi h \times 2h$) consisting of $N_x \times N_y = 60 \times 64$ cells. The height of the wall-adjacent grid cell is $\Delta y^+ \approx 0.9$. The resolution of the uniformly distributed grid cells in streamwise and spanwise directions corresponds to $\Delta x^+ = 19.0$ and $\Delta z^+ = 18.0$ respectively. The fully-developed flow conditions are provided by applying periodic inlet-outlet boundary conditions.

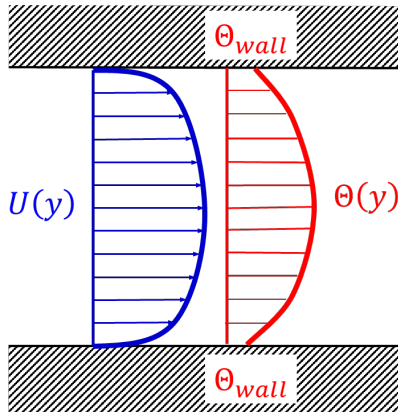


Figure 1: Schematic of the fully-developed channel flow

Fig. 2 schematically shows the flow domain adopted for the simulations of the round impinging jet. The jet structure corresponds to a fully-developed pipe flow at a diameter D -based Reynolds number of $Re = 10000$. The pipe-like round jet entering the flow domain is realized by a separate computation of a pipe segment by applying the periodic inlet/outlet conditions. The flow field thus generated is subsequently mapped onto the domain inlet. The jet generated in this way impinges perpendicularly on a partially heated wall situated at $2D$ distance from the pipe exit, with boundary conditions corresponding to a constant wall temperature. The solution domain having the form of a truncated cylinder, confined in the normal direction by the bottom wall and an upper confinement plate, extends to $12D$ in the radial direction. The grid detail in the radial $x-y$ plane is shown in Fig. 3. The number of the cells within the horizontal $x-y$ plane of $N_{x-y} = 46400$ multiplied by the $N_z = 138$ in the normal direction amounts 6.4 Million cells in total. The height of the wall-adjacent grid cell is $\Delta z^+ = 0.06 - 0.94$ (the lower values relate to the immediate impinging area and the higher values to the region close to the configuration outlet). The grid resolution in the radial direction corresponds to $\Delta r^+ = 4.76 - 139.54$. The same three-dimensional solution domain and grid resolution have been applied for both conventional and Sensitized RANS simulations.

RESULTS AND DISCUSSION

As an illustration, Figures 4 and 5 display the instantaneous velocity and temperature fields in both considered configurations, plane channel and round impinging jet, obtained

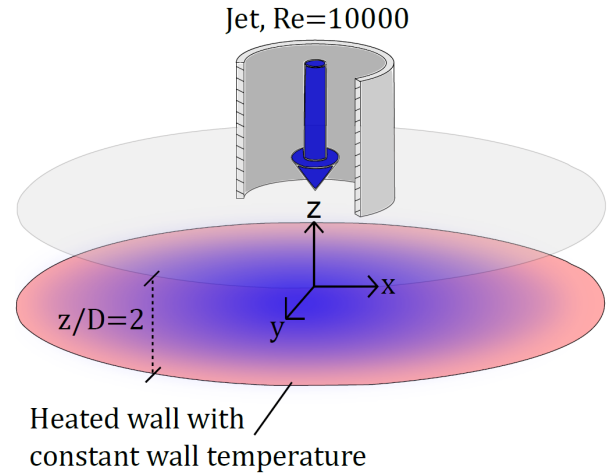


Figure 2: Schematic of the impinging jet configuration

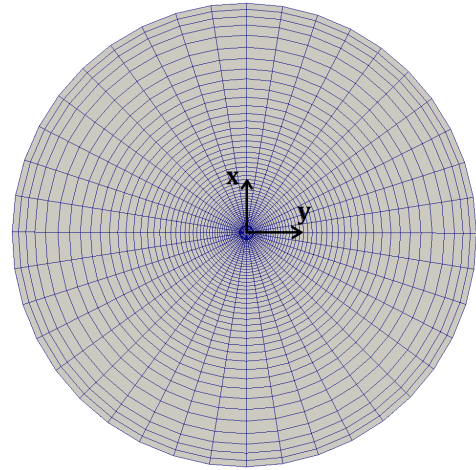


Figure 3: Detail of the numerical grid in the radial $x-y$ plane for the impinging jet configuration

by the IIS-RSM. In both cases the temperature difference between the working fluid and the heated/cooled wall is 10°C . The temperature field is scaled to have zero values (temperature minimum) at both channel walls and the pipe exit and unit values (temperature maximum) at the channel symmetry plane and at the impinging wall. The scale-resolving capabilities of the IIS-RSM are clearly evident at both flow fields exhibiting turbulent fluctuations. The dynamics of both velocity and temperature fields is mainly driven by their resolved fractions generated via the convective terms in the corresponding transport equations. However, in the wall proximity, the sub-scale turbulent momentum and heat fluxes are adequately enhanced and are therefore crucial for capturing correctly the near-wall effects. In the following individual sections some time-averaged mean flow and turbulence properties will be discussed along with the reference DNS results.

Channel flow

Figures 6 illustrate the mean velocity and Reynolds stress component profiles obtained by both RANS-RSM and IIS-RSM across the fully-developed channel flow. Apart from a slight underprediction of the peak value of the streamwise stress component u^2 and a certain overprediction of the spanwise stress component w^2 , the results obtained show very good

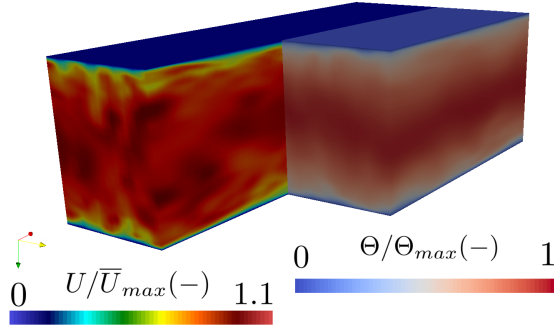


Figure 4: Instantaneous velocity and temperature fields in a turbulent channel flow with fixed wall temperature obtained by the IISRSM

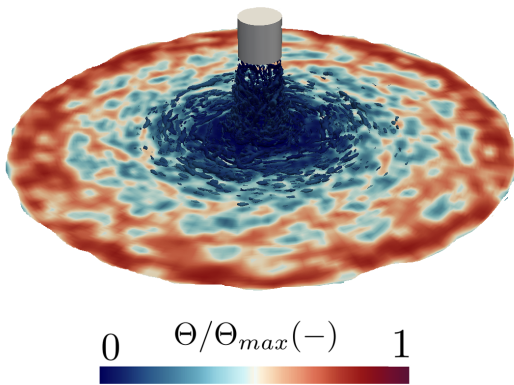


Figure 5: Flow visualization by the Q -criterion, colored by the instantaneous temperature field in a turbulent impinging jet with fixed wall temperature obtained by the IISRSM

agreement with the DNS database in all characteristic boundary layer zones, viscous sublayer, buffer zone and the logarithmic region. Considering a passive character of the temperature field, there is no relevant influence on the mean velocity and turbulence field. Accordingly, the use of different heat flux models is irrelevant here. Similar good agreement with the DNS reference is reported with respect to the mean temperature profile, Fig. 7. The influence of the SGDH (Eq. 6) and GGDH (Eqs. 7-8, with $C_{\theta,1} = 0.3$ and $C_{\theta,2} = 0$) heat flux model formulations on the temperature profile development is not noticeable. Considering that both heat flux formulations were applied in conjunction with a full Reynolds stress RANS model, for which a correctly predicted Reynolds stress field representing the constituent of the relevant gradient diffusion coefficients was used, this outcome is not very surprising. On the other hand, this was anyhow expected for the IISRSM application, given the appropriate level of the resolved turbulence. The modeled heat flux relates here only to the residual sub-scale motion. Accordingly, only the results of the GGDH formulation is shown in conjunction with the eddy-resolving RSM version.

Impinging jet

Figures 9 depict the iso-contours of the time-averaged velocity field including mean flow streamlines. The mean flow topology reveals a flow pattern typically characterizing

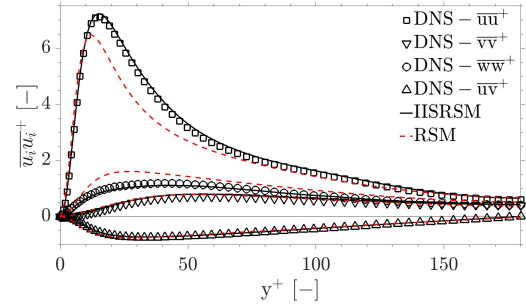
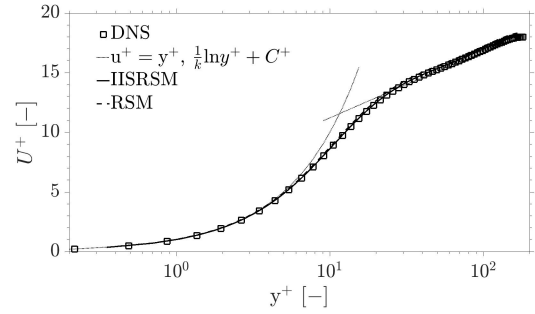


Figure 6: Mean velocity and Reynolds stress component profiles in the fully-developed channel flow

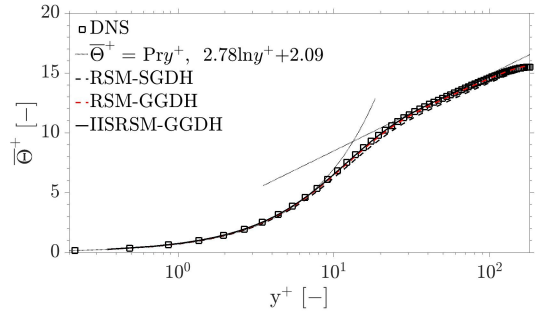


Figure 7: Mean temperature profile in the fully-developed channel flow

impinging jet configurations featured by an intensive alternation in the velocity gradient, from abrupt jet deceleration in the immediate impingement area toward a prompt 90° flow skewing and transition into the wall-jet region followed by a strong acceleration and subsequent flow relaxation. It is furthermore well known that a streamline curvature-induced turbulence production takes place here, which represents an inherent feature of Reynolds stress modeling group, but on the other hand is beyond the reach of the eddy-viscosity modeling concept. Due to the upper confinement plane (see Fig. 2), a flow reversal of weak intensity is generated above the wall jet region.

Figures 10 illustrate the computationally, by IISRSM and RSM, obtained semi-log profile development of the mean velocity magnitude, Reynolds stress components and temperature at selected locations within the flow domain along with the DNS reference results. The vertical coordinate is logarithmically scaled to emphasize the near-wall behavior of the flow quantities considered. Herewith, a detailed quantitative assessment of the results quality is enabled. The velocity profiles are characterized by a flow momentum intensification occurring during the impingement event (at $r/D = 0.5 - 1.0$) and subsequent transition (at $r/D \geq 1.0$) into the wall jet. After-

ward the flow momentum weakens appropriately. Agreement with the DNS database is remarkable, especially concerning the IISRSM results. The RSM-related results shows also a reasonable level of agreement with DNS. It can be said, considering the large departures of the RSM-specific Reynolds stress components, that the latter behavior is mainly due to the role of the mean pressure gradient which dominates the balance in the equation of motion, overcoming significantly the Reynolds stress gradients. The radial (parallel to the impinging plate) $\overline{u_r u_r}$ and shear $\overline{u_r u_z}$ stress components returned by the IISRSM follow closely the DNS database. At the cross-section $r/D = 0.5$, which coincides with the pipe outlet, the maxima of both stress components originate from the near-wall region within the pipe. The correctly predicted double maximum at the $\overline{u_r u_r}$ component, visible at $r/D = 1.0 - 2.0$, coincides with the wall-jet boundary characterized by a velocity maximum at $z/D = 0.1$ and the strong mean shear in the immediate vicinity of the wall at $z/D = 0.01$. The RSM Reynolds stress profiles reveal significant overprediction in the direct impingement area at $r/D = 0.5$ and 1.0 . This can be partially explained by the 'standard' expression of the so-called wall-reflection redistribution term that features the present RSM, which was originally formulated for wall-parallel flows (see Craft *et al.* (1993) for a related discussion). The difference in the performance of two tested heat flux models, SGDH and GGDH, is visible at the temperature profiles, although a clear superiority of any of the applied models cannot be clearly established. Small differences in the wall temperature gradients are reflected in the distribution of the Nusselt number displayed in Fig. 8. A characteristic second peak at $r/D \approx 2$, apart of that related to the impingement center (at $r/D = 0$), is returned by all models despite an obviously flattened Nu -distribution at this position. The RSM-related enhanced peak at $r/D = 0$ is due to increased turbulence intensity in the immediate impingement location. The IISRSM-specific underprediction requires a more detailed analysis also with respect to the grid resolution requirements, considering that the standard grid resolution constraints are primarily derived for the wall-parallel flows (see e.g., Hadžiabđić & Hanjalić (2008)).

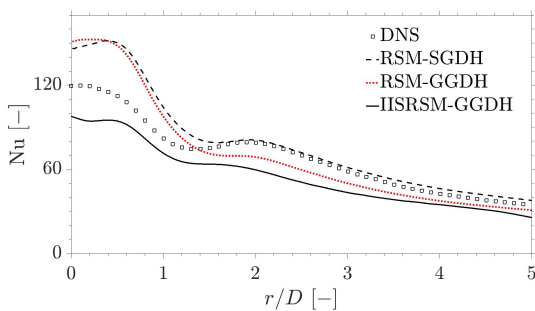


Figure 8: Nusselt number distribution at the impinging wall

CONCLUSIONS

The predictive performance of heat flux ($\overline{u_j \theta'}$) modeling in conjunction with passive scalar transport in a plane channel and an impinging jet flow configuration was studied presently. The results obtained by applying the RANS Reynolds stress model and its eddy-resolving variant denoted by IISRSM show a high degree of consistency. The turbulence level overprediction pertinent to the central impingement region obtained by the RSM could be significantly improved by utilizing the corresponding model version with the enhanced capability of accounting for turbulence unsteadiness. Pronounced differences

in the thermal field results with respect to the application of the SGDH and GGDH models were not revealed this time, because the background Reynolds stress model of turbulence used in conjunction with both heat flux model expressions, provided a qualitatively valuable coefficient prediction in both gradient-diffusion approaches tested.

Acknowledgments

The financial support of the German Research Foundation (DFG) in the framework of the Collaborative Research Center/Transregio 150 (SFB-TRR 150, Project Number 237267381) is gratefully acknowledged. The authors furthermore would like to thank for the computing time granted on the Lichtenberg HPC at TU Darmstadt.

REFERENCES

- Abe, K. & Suga, K. 2001 Towards the development of a Reynolds-averaged algebraic turbulent scalar-flux model. *Int. J. Heat and Fluid Flow* **22**, 19–29.
- Chang, K.-C. & Shyu, M.-J. 2000 Revisiting the Reynolds-averaged energy equation in near-wall turbulence models. *Int. J. Heat and Mass Transfer* **43**, 665–676.
- Craft, T.J., Graham, L.J.W. & Launder, B.E. 1993 Impinging jet studies for turbulence model assessment - ii. an examination of the performance of four turbulence models. *Int. J. Heat and Mass Transfer* **36**(10), 2685–2697.
- Hadžiabđić, M. & Hanjalić, K. 2008 Vortical structures and heat transfer in a round impinging jet. *Journal of Fluid Mechanics* **596**, 221–260.
- Horiuti, K. 1992 Assessment of two-equation models of turbulent passive-scalar diffusion in channel flow. *Journal of Fluid Mechanics* **238**, 405–433.
- Jakirlić, S. & Hanjalić, K. 2002 A new approach to modelling near-wall turbulence energy and stress dissipation. *Journal of Fluid Mechanics* **459**, 139–166.
- Jakirlić, S. & Maduta, R. 2015 Extending the bounds of 'steady' RANS closures: Toward an instability-sensitive Reynolds stress model. *Int. J. Heat and Fluid Flow* **51**, 175–194.
- Jakirlić, S. & Maduta, R. 2016 Sensitized-RANS modelling of turbulence: Resolving turbulence unsteadiness by a (near-wall) Reynolds stress model. In *Progress in Wall Turbulence 2* (ed. M. Stanislas *et al.*), pp. 17–35. Springer.
- Kasagi, N., Horiuti, K., Miyake, Y., Miyauchi, T. & Nagano, Y. 1992 Establishment of the direct numerical simulation data bases of turbulent transport phenomena. Co-operative Research No. 02302043. Supported by the Ministry of Education, Science and Culture, <https://tthlab.jp/DNS/CH122.PG.WL3>.
- Menter, F.R. & Egorov, Y. 2010 The scale-adaptive simulation method for unsteady turbulent flow predictions. part I: theory and model description. *Flow, Turbulence and Combustion* **85** (1), 113–138.
- Rotta, J.C. 1972 *Turbulente Strömungen. Eine Einführung in die Theorie und ihre Anwendung*, 1st edn. Teubner Verlag Stuttgart.
- Secchi, F., Häber, T., Gatti, D., Schulz, S., Trimis, D., Suntz, R. & Frohnappfel, B. 2022 Turbulent impinging jets on rough surfaces. *GAMM, Special Issue on Direct Numerical Simulations of Turbulent Flows - Part I* **45**.
- Šarić, S. & Basara, B. 2018 A near-wall model for heat transfer at high Prandtl numbers. In *International Conference on Computational Fluid Dynamics (ICCFD10), Barcelona, Spain, July 9-13*.

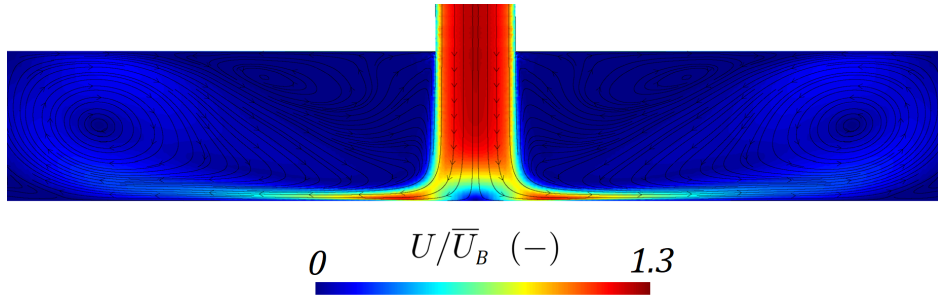


Figure 9: Iso-contours of the time-averaged velocity field with associated mean flow streamlines in the impinging jet configuration obtained by the IISRSM

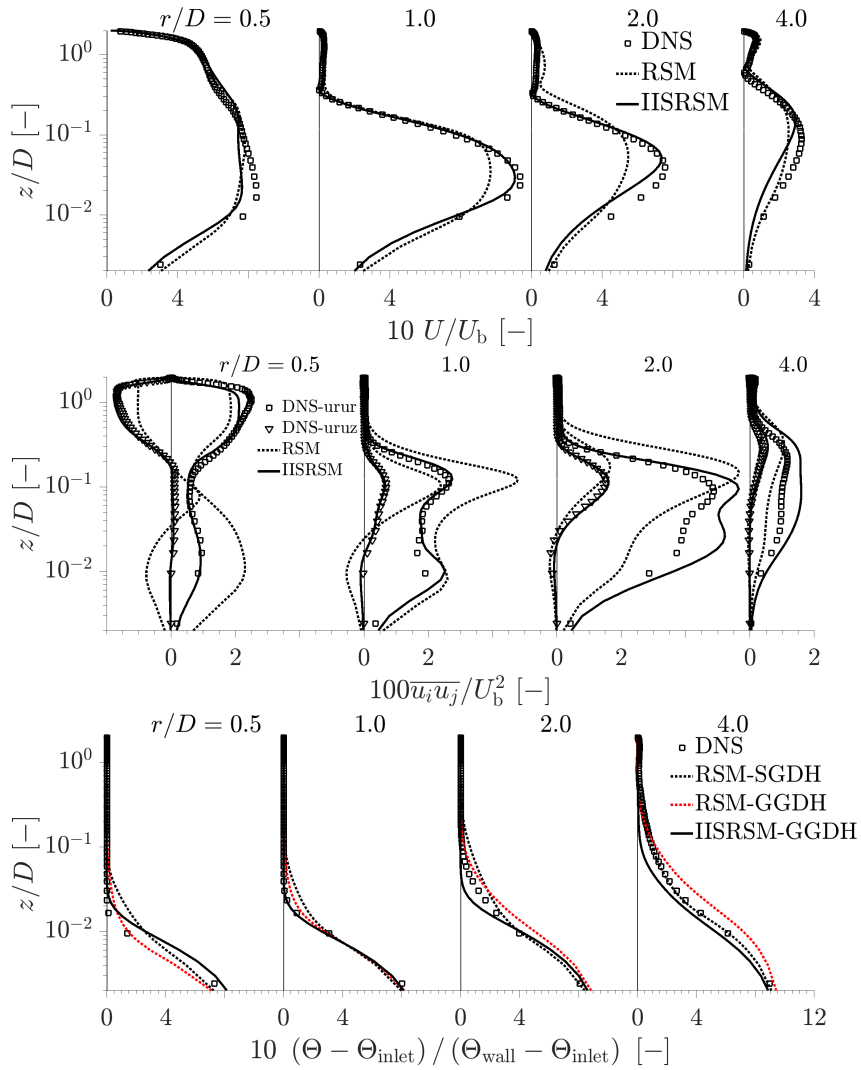


Figure 10: Profile development of the mean velocity magnitude, radial and shear stress components and mean temperature in the impinging jet configuration